

Article

Modification of Magnetic Graphene Oxide by an Earth-Friendly Deep Eutectic Solvent to Preconcentrate Ultratrac Amounts of Pb(II) and Cd(II) in Legume Samples

Melika Hejazikhah and Parastoo Jamshidi *

School of Chemistry, College of Science, University of Tehran, Tehran P.O. Box 14155-6455, Iran

* Correspondence: parastoo.jamshidi@ut.ac.ir

Abstract: A novel magnetic solid-phase extraction adsorbent using deep eutectic solvent-coated magnetic graphene oxide (EgLiCl-mGO) was proposed for simultaneous preconcentration of Pb(II) and Cd(II). The nanocomposite was characterized by Fourier Transform Infrared Spectroscopy, X-ray diffractometry, and alternative gradient force magnetometer. Parameters that could affect the preconcentration recoveries of the target ions were investigated via the one-factor-at-a-time method. The optimum conditions are pH of 4 ± 0.5 , EgLiCl-mGO amount of 1.0×10^{-2} g, adsorption time of 5 min, eluent of HNO₃ (1 mL, 2 mol L⁻¹), and desorption time of one minute. The swelling property of the adsorbent versus pH was studied. The linearity of the dynamic range for Pb(II) (5.0×10^{-6} – 4.0×10^{-4} g L⁻¹) and Cd(II) (5.0×10^{-6} – 15×10^{-5} g L⁻¹) was recorded. The limits of detection were Pb(II): 1.2×10^{-6} g L⁻¹ and Cd(II): 47×10^{-8} g L⁻¹. The preconcentration factor of 50 was calculated for both ions and the relative standard deviations were 1.27% for Pb(II) and 0.94% for Cd(II). Reusability, effect of interference ions, selectivity, isotherm adsorption, kinetic adsorption, and thermodynamic adsorption were established. The adsorbent was successful at preconcentrating the ions in legumes.



Citation: Hejazikhah, M.; Jamshidi, P. Modification of Magnetic Graphene Oxide by an Earth-Friendly Deep Eutectic Solvent to Preconcentrate Ultratrac Amounts of Pb(II) and Cd(II) in Legume Samples. *Appl. Sci.* **2023**, *13*, 5702. <https://doi.org/10.3390/app13095702>

Academic Editor: Adina Magdalena Musuc

Received: 13 December 2021

Accepted: 11 August 2022

Published: 5 May 2023

Publisher's Note: MDPI stays neutral with regard to jurisdictional claims in published maps and institutional affiliations.



Copyright: © 2023 by the authors. Licensee MDPI, Basel, Switzerland. This article is an open access article distributed under the terms and conditions of the Creative Commons Attribution (CC BY) license (<https://creativecommons.org/licenses/by/4.0/>).

Keywords: deep eutectic solvent; MSPE; Pb(II); Cd(II); legumes; flame atomic adsorption spectroscopy

1. Introduction

Deep eutectic solvent (DES) has received attention in the recent years. DES is an emerging class of safe materials related to ionic liquid (IL), which has abnormally deep melting point depression at the eutectic mixture of specific hydrogen bond donors (HBDs) and acceptors (HBAs). DESs are divided into five categories depending on the method of preparation [1,2]. Type I is composed of a quaternary ammonium salt and a metal chloride, Type II is a mixture of a quaternary ammonium salt and a metal chloride hydrate, Type III is a mixture of a quaternary ammonium salt and an HBD, Type IV consists of a metal chloride hydrate and an HBD, and Type V consists of only nonionic, molecular HBAs and HBDs. All types of DESs have high thermal stability, low volatility, low vapor pressure, and tunable polarity. Their preparation does not need any extra solvent so no purification step is needed. Therefore, they are applicable substitutions for volatile organic compounds (VOCs), used widely throughout research and industry with the aim of environmental remediation, especially magnetic solid-phase extraction (MSPE) [3–5].

MSPE is a developed generation of solid-phase extraction, which uses magnetic or magnetically modified adsorbents to extract analytes with high efficiency. This tactic overcomes some weak points in solid-phase extraction such as decreasing the time of preconcentration, sample loading, and filtration or centrifugation steps [6–8]. Magnetic graphene oxide is an example of an MSPE adsorbent. Graphene oxide (GO) is a fascinating new class of two-dimensional carbon nanostructures. It has high surface area, good chemical stability, and strong thermal stability. GO contains hydroxyl, epoxide, carboxyl, and carbonyl functional groups; additionally, its hydrophilic property increases its negative

charge and dispersibility in aqueous solution to form a stable suspension. GO has strong interaction with magnetic nanoparticles; accordingly, mGO can be a good candidate to be applied MSPE as an adsorbent. GO can be functionalized with organic components via π - π interaction to control selective adsorption of analyte(s) [9–12]. DES is an example, which can be a modifier, disperser, and fictionalizer for mGO.

Many scientists have used DES to improve the extraction or preconcentration methods. For example, a DES of ethylene glycol and ammonium-based salt functionalized carbon nanotube to adsorb methyl orange from aqueous solution [13]. Additionally, a novel DES was applied as a modifier for graphene and graphene oxide to remove chlorophenols [14]. In addition to organic materials, DES can be a qualified candidate to adsorb cations such as heavy metals, because it has active negative sites and can grab cations via electrostatic force [15].

In this study, magnetic graphene oxide modified with DES (EgLiCl-mGO) was applied as an efficient nano-adsorbent for preconcentrating Pb(II) and Cd(II) simultaneously in legume samples. Pb(II) and Cd(II) are toxic elements and their accumulative characters cause serious problems for humans, plants, and animals [16]. According to specific properties of EgLiCl-mGO, it could be a highly applicable adsorbent. mGO facilitates the preconcentration procedure because graphene oxide has a high surface area and magnetic properties enable easy and fast separation of EgLiCl-mGO [7,17–20]. The presence of DES provided a wide surface area with functional groups, which has a synergistic effect on adsorption efficiency. More importantly, EgLiCl is inexpensive, biodegradable, nontoxic, and easy to prepare. For the evaluation of the effective variables on the preconcentration efficiency, the one-at-a-time method was employed and pH, adsorption time, adsorbent amount, desorption time, and kind of eluent were optimized. Analytical figures of merit, interference effect of various ions, reusability, swelling behavior, adsorption isotherm, adsorption kinetics, and adsorption thermodynamics were reported. Finally, the target analytes were analyzed in the four different legumes.

2. Materials and Methods

2.1. Apparatus

Absorbance quantifications of Pb(II) and Cd(II) were conducted using a flame atomic absorption spectrometer (FAAS; Younglin Aas 8020 (<http://youngin.com>, Gyeonggi, South Korea)) with a deuterium background correction system and an air-acetylene burner. All pH adjustments were conducted with a digital pH meter (Metrohm—827 (www.metrohm-ag.com, Herisau, Switzerland)). The instrument has a glass combination electrode. The X-ray powder diffraction pattern (XRD; Philips—PW1730 (www.panalytical.com, Eindhoven, The Netherlands)) was obtained under the Cu-K α radiation (1.2 kW). 2θ ranged from 10° to 80° , scan step and step time were 0.05° and 1 s, respectively. An alternative gradient force magnetometer (AGFM; Meghnatis Daghhigh Kavir Company (<https://nano.kashanu.ac.ir>, Kashan, Iran)) measured magnetic properties in an applied magnetic field sweeping between $\pm 10,000$ Oe. Fourier transform infrared spectra (FT-IR; ABB Bomem MB100 (<http://new.abb.com>, Zürich, Switzerland)) were recorded over the range 400–4000 cm^{-1} .

2.2. Reagent and Solution

All the reagents were of analytical grade. The standards of Pb(II) and Cd(II) (1.0×10^{-3} g L $^{-1}$) were prepared using their nitrates salts. Flake graphite, P $_2$ O $_5$, H $_2$ SO $_4$, K $_2$ S $_2$ O $_8$, H $_2$ SO $_4$, KMnO $_4$, NaNO $_3$, HCl, H $_2$ O $_2$, FeCl $_3 \cdot 6$ H $_2$ O, FeCl $_2 \cdot 4$ H $_2$ O, NH $_4$ OH, ethylene glycol (Eg), and LiCl were procured from Merck Company (www.merck.de, Darmstadt, Germany). Ultra-high purity water from a Milli-Q system was used to prepare sample solutions.

2.3. Synthesis

Graphene oxide (GO) was prepared using the modified Hummer's method. A mixture of flake graphite (4.0×10^{-3} g), H_2SO_4 (12 mL), and P_2O_5 (8×10^{-3} g) was magnetically stirred for 6 h and then filtered. Afterwards, H_2SO_4 (12 mL) and $\text{K}_2\text{S}_2\text{O}_8$ (8.0×10^{-3} g) were added to the filtrate and was magnetically stirred for 6 h. The materials were cooled to room temperature, eluted by deionized water (300 mL), dried at room temperature, and then heated at 60°C for 2 h. Pre-oxidized graphite powder (2.0×10^{-3} g), H_2SO_4 (92 mL), and KMnO_4 (12×10^{-3} g) were stirred together in an ice bath. After 15 min, NaNO_3 (2.0×10^{-3} g) was added to the materials and was stirred at room temperature for 2 h. Then deionized water (200 mL) was added and stirred for 15 min. H_2O_2 (30%, 10 mL) and distilled water (500 mL) were added. The materials were filtered and washed using HCl (10%) to reach the brown suspension, and then they were heated at 60°C for 30 min. The cooled materials were sonicated in H_2O_2 (10%, 10 mL) for 5 min. The yellow-brown residual powder was washed with warm deionized water 3 times to remove the impurities. GO was dried at 60°C [21,22].

Secondly, a magnetic carbonic nanocomposite was synthesized based on Massart's method. Deionized water (100 mL), $\text{FeCl}_3 \cdot 6\text{H}_2\text{O}$ (2.5 g), $\text{FeCl}_2 \cdot 4\text{H}_2\text{O}$ (9.0×10^{-1} g), and GO (1.0×10^{-1} g) were sonicated for 15 min. Afterwards, under nitrogen atmosphere, NH_4OH (25%, 15 mL) was dripped to fix the pH~11. After stirring for 12 h, mGO was magnetically gathered, eluted using distilled water, and dried at 80°C [23].

Finally, Eg (5.0×10^{-2} g) and LiCl (5.0×10^{-2} g) were mixed together at 60°C . A colorless liquid shows a successful synthesis of DES. mGO (5.0×10^{-2} g) was dispersed into the DES via one hour sonication. The final product (EgLiCl-mGO) was eluted using deionized water and then dried at 30°C [24].

2.4. General Procedure

Pb(II) and Cd(II) (5.0×10^{-5} g L^{-1}) were dissolved in deionized water (50 mL). EgLiCl-mGO (1.0×10^{-2} g) was added into the sample solution at the pH of 4 ± 0.5 , followed by shaking for 5 min. EgLiCl-mGO was gathered magnetically. One-minute sonication in the presence of HNO_3 (1 mL, 2 mol L^{-1}) completed the process of preconcentration. Eluted ions were quantified by FAAS.

2.5. Sample Preparation

Four different legume samples including kidney bean, cowpea, pinto bean, and navy bean were procured from local stores in Tehran, Iran. The samples were cleaned with deionized water. They were dried to reach the stable weight, and then cooled to room temperature. The samples (1.0×10^{-1} g) were transferred into a Teflon vessel containing HNO_3 (15 mL, 65%), and kept immersed for 48 h. The digestion heating steps are reported below: Firstly, the temperature was raised to 90°C in 10 min and stayed for 5 min. Then, the temperature increased to 150°C and remained for 10 min, followed by adding H_2O_2 (20 mL, 30%). Finally, the vessels were cooled down to room temperature. The solution in each vessel was transferred to a polyethylene volumetric flask and diluted to 100 mL. The pH of two separate 50 mL aliquots of digested samples was adjusted to 4 ± 0.5 using HNO_3 and NH_3 solutions. The general procedure was applied as mentioned in Section 2.4. Matrix spiking with standards of Pb(II) and Cd(II) (5.0×10^{-5}) was employed to evaluate the effect of the matrix.

3. Results

3.1. Characterization

FT-IR spectra confirm that Eg-LiCl was loaded onto mGO completely (Figure 1). The FT-IR spectrum of mGO was drawn in the orange spectrum. The stretching O-H, carbonyl C=O, aromatic C=C, bending O-H, aromatic C-C, alkoxy C-O-C, stretching CH_2 , and carbonyl C=O bonds are identified according to the peaks of 3380, 1730, 1630, 1360, 1220, 1050, 2880, and 1730 cm^{-1} , respectively. Peaks lower than 700 cm^{-1} characterize

bonds of Fe–O [25]. The blue spectrum is related to EgLiCl-mGO. The bands of 3430 and 1640 cm^{-1} are associated O–H bonding. Alkane CH_2 stretching, CH_2 scissor, CH_2 wagging, and CH_2 twisting are characterized according to peaks around 2914, 1460, 1350, and 1258 cm^{-1} , respectively. The sorption peaks of Li–O and Fe–O were seen at the wavelengths of 1300 and 700 cm^{-1} , respectively [25]. Table S1 summarizes the data.

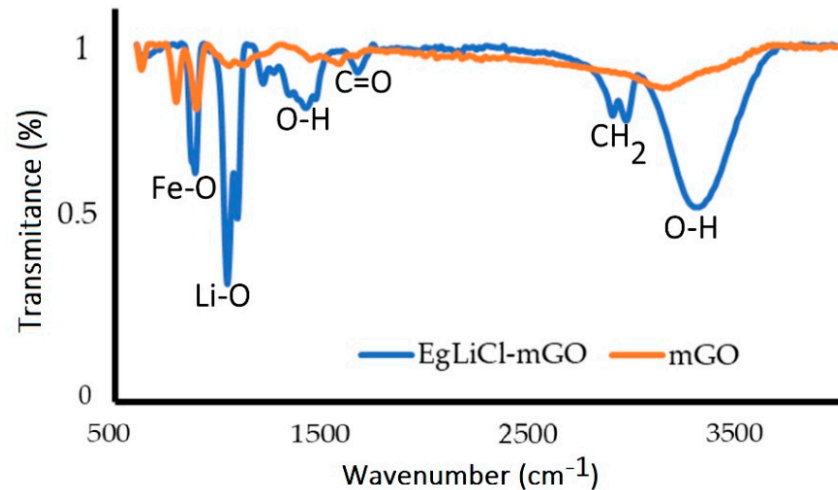


Figure 1. FT-IR spectra of mGO and EgLiCl-mGO.

The X-ray diffraction (XRD) analysis of EgLiCl-mGO is patterned in Figure 2a, which has good agreement with JCPDS cards No. 01-075-0449, indicating magnetite Fe_3O_4 and JCPDS cards No. 01-079-1715 confirming the GO structure. Fe_3O_4 was characterized by peaks at 30.70, 35.97, 37.23, 43.74, 53.94, 57.55, 63.32, and 67.14°. Additionally, peaks at 11.23, 21.64, 30.70, 35.97, 43.74, 53.94, 57.55, 63.32, and 75.08° are related to GO [26]. The process of loading EgLiCl onto mGO broadened the peaks of mGO. The crystal size of the total product was calculated using the Scherrer formula. It is about 6 nm.

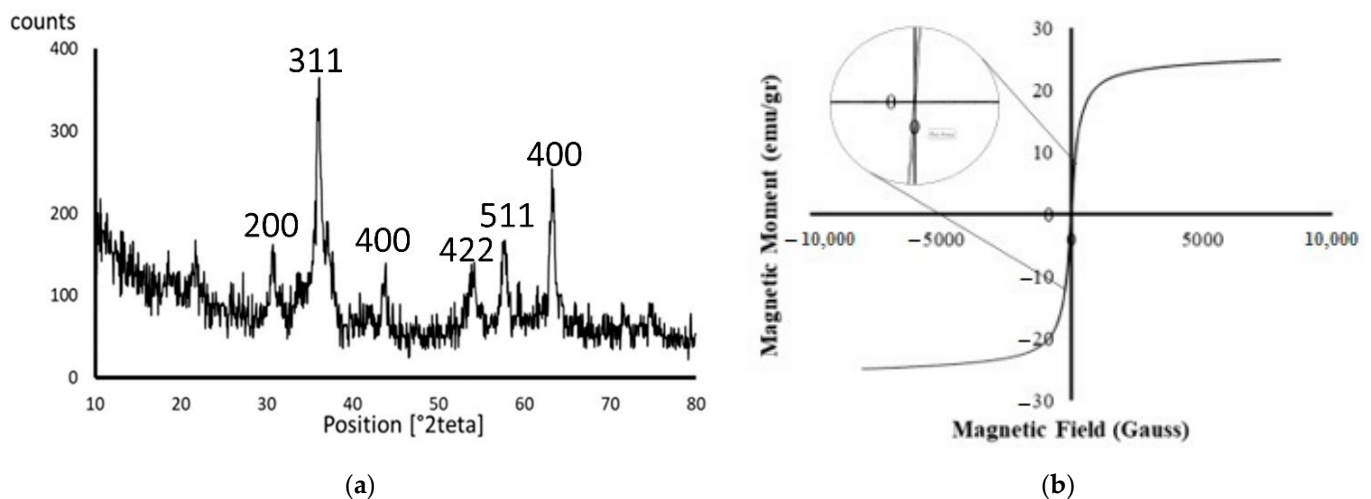


Figure 2. (a) The XRD pattern of EgLiCl-mGO; (b) magnetic hysteresis loops image of EgLiCl-mGO.

The AGFM curve of EgLiCl-mGO is presented in Figure 2b. The amount of ± 25 electromagnetic units (emu g^{-1}) is helpful for the rapid gathering of the adsorbent in the sample solution [27]. The remanent magnetization is almost zero, confirming the superparamagnetic property and the presence of Fe_3O_4 nanoparticles.

3.2. Optimization of the Method

3.2.1. Effect of pH

Alkaline or acidic condition of samples plays a crucial part for the preconcentration of heavy metals by solid adsorbents because it has a direct effect on Pb(II) and Cd(II) ion retention on the negative sites of EgLiCl-mGO. It may be possible for the cations to form coordination compounds with oxygen groups via electrostatic force. Recovery of the investigated ions on the EgLiCl-mGO was found Pb(II): 99.1 and Cd(II): 98.4 in pH of 4 ± 0.5 . Quantitative recovery values were found in the pH range of 2–9. After pH~5, recovery values of the preconcentrated ions decreased because heavy metal ions were hydrolyzed with formation of metal hydroxides. Therefore, pH~4 was applied as the optimized pH value for further experiments. Additionally, in highly acidic pH, the negative active sites will be occupied by H^+ sooner than the target cations.

3.2.2. Effect of Adsorption Time

A certain period of time must pass to reach a complete adsorption. Accordingly, a fixed amount of EgLiCl-mGO was added to the sample solutions of Pb(II) and Cd(II) (50 mL, $5.0 \times 10^{-5} \text{ g L}^{-1}$) under the adsorption time, ranging from 1 to 30 min. The experiment results show that the performance of the method has increasing trend from 1 to 5 min, but after that there are slight differences in the recoveries. Therefore, the adsorption time of 5 min was selected for the next experiments.

3.2.3. Effect of Adsorbent Amount

An appropriate amount of adsorbent is an essential parameter in the MSPE method. On the one hand, this is effective for the usage amounts of materials; on the other hand, it provides sufficient active sites for adsorption of target analytes. In this context, the influence of EgLiCl-mGO amount on the simultaneous preconcentration efficiencies of Pb(II) and Cd(II) remained constant with the adsorbent amount ranging from 1.0×10^{-2} to $5.0 \times 10^{-2} \text{ g}$. This indicates high affinity of EgLiCl-mGO toward these heavy metals. Therefore, $1.0 \times 10^{-2} \text{ g}$ was selected for the next step of optimization.

3.2.4. Effect of Eluent Type

The influence of the eluent type on the simultaneous preconcentration efficiency of Pb(II) and Cd(II) by EgLiCl-mGO was compared in the presence of two acids (Table 1). The highest analytical yields for the target analyte were observed using HNO_3 (2 mol L^{-1}). Afterwards, the volume influence of HNO_3 on the extraction efficiency of the target analytes was studied in the range of 0.5–2 mL. The efficiency remained stable in all volumes. As one of the concerns in this article is using the minimum amounts of materials with the maximum performance, 1 mL was selected as the optimum volume of eluent.

Table 1. Results of different eluents (1 mL) on the preconcentration of Pb(II) and Cd(II) (n = 3).

Recovery (%)		Eluent
Cd(II)	Pb(II)	
60.52 ± 0.03	41.23 ± 0.01	HNO_3 (1 mol L ⁻¹)
98.14 ± 0.05	99.34 ± 0.07	HNO_3 (2 mol L ⁻¹)
84.48 ± 0.11	76.15 ± 0.13	HNO_3 (5 mol L ⁻¹)
14.96 ± 0.10	24.94 ± 0.14	HCl (1 mol L ⁻¹)
22.46 ± 0.15	11.16 ± 0.11	HCl (2 mol L ⁻¹)
5.63 ± 0.08	4.63 ± 0.11	HCl (5 mol L ⁻¹)

3.2.5. Effect of Desorption Time

A completion of the desorption step depends on the desorption time. Insufficient desorption time does not let the eluent elute the adsorbed ions, resulting in poor analytical efficiency of the method. At the same time, it has a direct effect on the speed of preconcentration.

tration. Therefore, it is necessary to find the optimum desorption time. In the present study, the effect of desorption time on the method was studied in the range of 1–5 min and 1 min of shaking is sufficient for desorption of Pb(II) and Cd(II).

3.3. Swelling Behavior of EgLiCl-mGO

The swelling behavior of the adsorbent in different pH was investigated through the recording of the swelling ratio of EgLiCl-mGO in aqueous solution (50 mL) of Pb(II) ($5.0 \times 10^{-5} \text{ g L}^{-1}$) and Cd(II) ($5.0 \times 10^{-5} \text{ g L}^{-1}$). A certain mass of the adsorbent ($1.0 \times 10^{-2} \text{ g}$) was shaken into sample solution at different pH (ranging from 2 to 9) at 25 °C for 5 min. Then, the weights of the swelled adsorbent were recorded after decanting the water. The swelling ratio (SR) of the fibers was determined using Equation (1):

$$SR = \frac{W_s - W_d}{W_d} \quad (1)$$

where W_s and W_d represent the weight of the wet adsorbent in water and that of dry adsorbent. Additionally, the pH effect of the sample solution on the swelling ratio was explored by recording SR in different pH ranging from 2 to 9 (Table 2). By increasing pH from 2 to 4, the swelling has an increasing trend but after that decreased significantly [28–30]. In all pH, EgLiCl-mGO adsorbed molecules of water via electrostatic interaction but in pH~4 the adsorption of Pb(II) and Cd(II) reached their maximum. The ion adsorption causes swelling of the adsorbent, illustrating the ability of EgLiCl-mGO to adsorb heavy metals.

Table 2. Swelling behavior of EgLiCl-mGO to adsorb Pb(II) and Cd(II) at different pH.

pH	W_d ($\times 10^{-2} \text{ g}$)	W_s ($\times 10^{-2} \text{ g}$)	SD
2	1.0	1.7	0.7
3	1.0	6.3	5.3
4	1.0	9.3	8.3
5	1.0	8.2	7.2
6	1.0	7.9	6.9
7	1.0	6.0	5.0
8	1.0	3.1	2.1
9	1.0	2.1	1.1

3.4. Reusability of EgLiCl-mGO

First, EgLiCl-mGO ($1.0 \times 10^{-2} \text{ g}$) was shaken in an aqueous solution (50 mL) of Pb(II) ($5.0 \times 10^{-5} \text{ g L}^{-1}$) and Cd(II) ($5.0 \times 10^{-5} \text{ g L}^{-1}$) and the amounts of heavy metals ions in the eluent were determined using FAAS. Five consecutive cycles were completed according to the procedure in Section 2.4. The metal ion adsorption efficiencies decreased after the second cycle. The method is reusable for two times. This decrease is related to negative effect of eluent onto EgLiCl-mGO. Eluent impacts on EgLiCl and affect the interaction among the components.

3.5. Interference Effect of Various Ions and Selectivity of EgLiCl-mGO

The study of interference effects on the suggested method is important, because the adsorption of Pb(II) and Cd(II) ions may be influenced by other cations and anions; consequently, the performance of the method decreases [31]. Adsorption of the target ions by EgLiCl-mGO was conducted in the presence of higher amounts of other ions with respect to their applications in real samples. The $\pm 5\%$ was considered as the maximum tolerance limit and values smaller than this amount were acceptable. Table 3 summarizes the data.

Table 3. The interfering effect of various ions on preconcentrating Pb(II) and Cd(II) (n = 3).

Ions	Ratio of Coexisting Ions	Recovery (%)	
		Pb(II)	Cd(II)
Na(I)	10,000	96.03 ± 0.12	98.14 ± 0.09
K(I)	10,000	98.12 ± 0.27	97.43 ± 0.11
Li(I)	800	99.17 ± 0.14	99.14 ± 0.08
Ca(II)	500	100.56 ± 0.21	99.17 ± 0.05
Mg(II)	300	98.08 ± 0.18	96.13 ± 0.04
Cr(II)	200	97.03 ± 0.24	99.94 ± 0.18
Pd(II)	800	97.26 ± 0.19	98.32 ± 0.11
Zn(II)	250	102.45 ± 0.11	100.32 ± 0.10
Al(III)	700	99.69 ± 0.27	98.71 ± 0.07
Mn(II)	500	97.34 ± 0.18	96.52 ± 0.04
Co(II)	100	98.98 ± 0.35	101.43 ± 0.01
Cu(II)	100	96.15 ± 0.28	96.83 ± 0.04
Ni(II)	100	95.28 ± 0.17	99.54 ± 0.9
SO ₄ ²⁻	1000	95.35 ± 0.31	98.18 ± 0.13
Cl ⁻	1000	97.53 ± 0.24	100.32 ± 0.15
NO ₃ ⁻	1000	99.18 ± 0.19	99.54 ± 0.09
CO ₃ ²⁻	1000	101.37 ± 0.20	100.91 ± 0.11

Under the optimum conditions, the selectivity of the method was studied. According to the data, the preconcentration efficiencies of Pb(II) and Cd(II) were 99% and 98%, respectively; however, the preconcentrating efficiencies of Cr(II), Cu(II), Mn(II), and Pd(II) were 32%, 85%, 17%, and 76%, respectively. This strength is related to selective interaction between target ions and specific active sites on the surface of EgLiCl-mGO. Pb(II) and Cd(II) have a smaller ionic radius so they have a greater charge density; consequently, they occupy the active sites of EgLiCl-mGO sooner and more strongly.

3.6. Sample Analysis

The accuracy of EgLiCl-mGO for simultaneous preconcentration of Pb(II) and Cd(II) in real samples was assessed through the spike method ($5.0 \times 10^{-5} \text{ g L}^{-1}$). Four different legumes including kidney bean, cowpea, pinto bean, and navy bean were purchased from local stores in Tehran, Iran. The sample preparation is explained in the section of sample preparation in detail, followed by applying the optimum procedure regarding Section 2.4. The results are presented in Table 4. The recovery values for the analyte ions were satisfactorily reasonable in the range 95–101%. The amounts of Pb(II) and Cd(II) were quantified in both the spiked and unspiked samples regarding Equation (2). The determination of ions was conducted using a FAAS.

$$R\% = \frac{C_1 - C_2}{C_3} \times 100 \quad (2)$$

where C_1 , C_2 , C_3 , and $R\%$ are spiked portion, unspiked portion, the amounts of the ions, and relative recovery, respectively.

3.7. Analytical Figures of Merit

Analytical figures of merit for the suggested procedure under the optimum conditions (Section 2.4) were determined from results of the analyses. The linear calibration equations for Pb(II) and Cd(II) were $A = 0.0011C + 0.0047$ (R^2 of 0.988) and $A = 0.0112C - 0.0172$ (R^2 of 0.998), respectively. Linearity of dynamic range (LDR) for Pb(II) (5.0×10^{-6} – $4.0 \times 10^{-4} \text{ g L}^{-1}$) and Cd(II) (5.0×10^{-6} – $15 \times 10^{-5} \text{ g L}^{-1}$) were recorded. In these equations, A is the absorbance of ions and C expresses as their concentrations in initial sample solutions. The limits of detection (LOD), expressed as $3S_b/m$ (S_b is blank standard deviation and m is slope of the calibration plot), were found as Pb(II) $1.2 \times 10^{-6} \text{ g L}^{-1}$ and Cd(II)

$47 \times 10^{-8} \text{ g L}^{-1}$ for five measurements of the blank. The limits of quantification (LOQ) were Pb(II) $3.9 \times 10^{-6} \text{ g L}^{-1}$ and Cd(II) $1.5 \times 10^{-6} \text{ g L}^{-1}$. LOQ was defined as 3.33 LOD. The preconcentration factor (PF) of 50 was calculated as the concentrations of ions before and after preconcentration. The reproducibility of the preconcentration method (relative standard deviation (RSD)) was determined by performing five experiments from solutions containing Pb(II) and Cd(II) (50 mL, $5.0 \times 10^{-5} \text{ g L}^{-1}$). The results showed 1.27% for Pb(II) and 0.94% for Cd(II).

Table 4. Analytical results of Pb(II) and Cd(II) quantified by EgLiCl-mGO (n = 3).

Sample	Spiked (g L ⁻¹)	Found	Recovery (%)	Found	Recovery (%)
		Cd(II)		Pb(II)	
Kidney bean	0	1.84	-	2.46	-
	5.0×10^{-5}	52.91	102.14	54.26	103.43
Cowpea	0	1.34	-	1.76	-
	5.0×10^{-5}	49.65	96.97	49.64	97.79
Pinto bean	0	3.11	-	2.95	-
	5.0×10^{-5}	51.98	97.87	50.75	95.84
Navy bean	0	0.95	-	4.76	-
	5.0×10^{-5}	52.04	102.15	54.38	99.30

Table 5 shows a comparison among EgLiCl-mGO with some new adsorbents. EgLiCl-mGO has an important development in MSPE including decreasing adsorbent amount and RSD as well as widening LDR. Additionally, EgLiCl-mGO was performed in semi-neutral pH, reducing the usage of materials to pH adjustment. More importantly, EgLiCl-mGO is a green, safe, and earth-friendly adsorbent and its preparation is fast without consumption of any dangerous material. The preconcentration time is about six minutes, which is another advantage of this method.

Table 5. Comparison of the proposed technique with several recent methods for simultaneous determination of heavy metals (FAAS was used for all detections).

Method	Amount (g)	LOD (g L ⁻¹)	RSD (%)	PF	LDR (g L ⁻¹)	Reference
SPE	-	6×10^{-6} – 12×10^{-6}	1.0–2.2	100	0.5×10^{-6} – 100×10^{-6}	[32]
MSPE	5.0×10^{-2}	0.06×10^{-6} – 0.76×10^{-6}	0.18–3.10	150	0.1×10^{-6} – 200×10^{-6}	[33]
LLE	-	0.38×10^{-6} – 0.42×10^{-6}	3.6–5.2	-	1.0×10^{-6} – 40×10^{-6}	[34]
SPE	4.0×10^{-3}	2.74×10^{-6} – 3.10×10^{-6}	3.2–3.5	50	-	[35]
SPE	-	0.031×10^{-6} – 0.043×10^{-6}	2.44–4.68	-	0.25×10^{-6} – 25×10^{-6}	[36]
MSPE	1.0×10^{-2}	47×10^{-8} – 1.2×10^{-6}	0.94–1.27	50	5.0×10^{-6} – $4.0 \times 10^{-4} \text{ g L}^{-1}$	This work

3.8. Adsorption Isotherm

The isotherm study shows the adsorption behavior of a system such as homogenous or heterogenous distribution of the analyte onto the surface of the adsorbent. In this article, five isotherm models were applied to investigate the adsorption of Pb(II) and Cd(II) on the surface of EgLiCl-mGO. This study was conducted in the presence of EgLiCl-mGO ($1.0 \times 10^{-2} \text{ g}$) in the sample solution containing the analytes (50 mL) during 5 min shaking at room temperature. According to Figure S1, increasing the initial concentration of ions has a direct effect on adsorption capacity (q_e) of EgLiCl-mGO, because by increasing C_e , q_e increases. q_e is calculated using the following equation.

$$q_e = \frac{(C_0 - C_e)}{W} \times V \tag{3}$$

C_0 is the initial concentration of the analyte, C_e is the equilibrium concentration of the analyte, V is the volume of the sample solution, and W is the amount of the adsorbent [37,38].

Langmuir is a monolayer adsorption model. It shows that the adsorbate molecules are adsorbed onto the homogeneous surface of the adsorbent. After the first layer of the analyte, no more analyte will be adsorbed onto the surface of the adsorbent. Equation (4) shows the linear form of this model.

$$\frac{1}{q_e} = \frac{1}{q_0 K_L C_e} + \frac{1}{q_0} \quad (4)$$

C_e is the equilibrium concentration of heavy metals adsorbed by EgLiCl-mGO, q_e is the retention capacity of analytes, K_L is the Langmuir constant, showing the binding energy between the adsorbate and adsorbent; q_{max} is the maximum adsorption capacity of the adsorbent. The straight line was obtained when $1/q_e$ was plotted against $1/C_e$ as shown in Figure S2. The slope and intercepts show the q_{max} and K_L , respectively [38–40].

The Freundlich model is a multilayer adsorption model. The linear form of the Freundlich model is written in Equation (5).

$$\ln q_e = \ln k_f + \frac{1}{n} \ln C_e \quad (5)$$

where K_f is the Freundlich constant, expressing the capacity, C_e defines the adsorbate concentrations of analytes, q_e is the quantity of ions at equilibrium, and n is the Freundlich exponent. K_f and n were determined from plot $\ln q_e$ vs. $\ln C_e$ (Figure S3). The n value shows the nature of adsorption ($1/n < 1$: normal process), ($1/n > 1$: cooperative process) [38–40].

The Temkin isotherm depicts the interaction between the adsorbate and the adsorbent and causes a linear decrease in the adsorption energy with surface coverage of the adsorbent. Equation (6) shows the linear form of this model.

$$q_e = \frac{RT}{B} \ln A_T + \frac{RT}{B} \ln C_e \quad (6)$$

where A_T is the Temkin isotherm equilibrium binding constant, R of $8.314 \times 10^3 \text{ J mol}^{-1} \text{ K}^{-1}$ is the universal gas constant, T is the absolute temperature, and B is the model constant and shows the heat of absorption [40,41]. Both B and A_T can be extracted from the plot q_e vs. $\ln C_e$ (Figure S4).

The Halsey isotherm model expresses the multilayer adsorption of the analyte over the heterosporous adsorbent. Equation (7) shows the linear form for the model.

$$\ln q_e = \left(\frac{1}{n_H}\right) \ln K_H - \left(\frac{1}{n_H}\right) \ln C_e \quad (7)$$

The Halsey isotherm model constant and Halsey isotherm model exponent are represented as K_H and n_H , respectively [38,40,41]. This model is plotted in Figure S5.

The Elovich model is based on multilayer adsorption, assuming exponential increasing trend in the adsorption sites as adsorption takes place. It is given by the equation below:

$$\ln\left(\frac{q_e}{C_e}\right) = \ln(K_e q_m) - \frac{q_e}{q_m} \quad (8)$$

K_e and q_m are the Elovich constants, representing the initial adsorption rate and maximum adsorption capacity, respectively [38,40,41]. Figure S6 shows the model.

Among the five mentioned models, Pb(II) follows the Freundlich model to be adsorbed onto EgLiCl-mGO, but Langmuir is fitted with the adsorption of Cd(II) onto EgLiCl-mGO. Therefore, the adsorption of Pb(II) onto the surface of EgLiCl-mGO is multilayered and a different layer of Pb(II) can be adsorbed onto each other but the adsorption of Cd(II) onto the surface of EgLiCl-mGO is the monolayer and after the first layer of Cd(II) no more

Cd(II) is adsorbed. Isotherm parameters of each model are summarized in Table 6. R^2 shows the best model for each of analyte. All the figures (Figures S1–S6) are plotted in the Electronic Supplementary Materials (ESMs).

Table 6. Adsorption isotherms for Pb(II) and Cd(II) onto EgLiCl-mGO.

Model	Pb(II)		Cd(II)	
	Parameters	R^2	Parameters	R^2
Langmuir	$q_0 = 75.18$ $K_L = 2.83$	0.99	$q_0 = 50$ $K_L = 1.45$	0.90
Freundlich	$n = 4.52$ $K_f = 45.36$	0.89	$n = 2.48$ $K_f = 24.77$	0.99
Temkin	$B = 233.31$ $A_T = 100.48$	0.92	$B = 178.38$ $A_T = 7.02$	0.93
Elovich	$q_m = 1.51$ $K_E = 727.18$	0.86	$q_m = 25.1$ $K_E = 2.76$	0.90
Halsey	$n = -4.52$ $K_H = 31.6 \times 106$	0.86	$n = -2.4$ $K_H = 2.9 \times 103$	0.97

3.9. Adsorption Kinetics

The rate and the characteristics of the adsorption of target analytes onto EgLiCl-mGO were investigated via pseudo-first-order and pseudo-second-order models. The samples of heavy metals (50 mL, 20 mg L⁻¹) were prepared and EgLiCl-mGO (1.0 × 10⁻² g L⁻¹) was added. The adsorption of ions was followed up at different time points, ranging from 1 to 60 min at room temperature.

The pseudo-first-order kinetic modeling is provided in the following equation:

$$\ln(q_e - q_t) = \ln q_{\max} - k_1 t \quad (9)$$

q_t (mg g⁻¹) and k_1 (min⁻¹) are the amounts of adsorbed ions onto EgLiCl-mGO at several times and the pseudo-first-order kinetic, respectively [42–45]. Figure S7 shows the plot.

The pseudo-second-order kinetic is plotted according to Equation (10).

$$\frac{t}{q_t} = \frac{1}{k_2 \times q_{cal}^2} + \frac{1}{q_{cal}} \times t \quad (10)$$

where q_t (mg g⁻¹) and k_2 (g mg⁻¹ min⁻¹) are the amount of adsorbed analyte onto the surface of solid adsorbent at various times and the rate constant of the pseudo-second-order kinetic, respectively [42,43]. Figure S8 shows the plot.

Figures S7 and S8 are presented in the Electronic Supplementary Materials (ESMs). The R^2 of the pseudo-first-order model was in the scope of 0.99 for both ions so the adsorption rate-controlling step was performed by occupying empty adsorption sites of EgLiCl-mGO by Pb(II) and Cd(II) (Table 7) [44–46].

Table 7. Comparison of kinetic models for Pb(II) and Cd(II) adsorption onto EgLiCl-mGO.

Analyte	Model	Parameters	Values	R^2
Pb(II)	Pseudo first order	k_1 (min ⁻¹) q_e (mg g ⁻¹)	0.03 95.40	0.99
	Pseudo second order	k_2 (g mg ⁻¹ min ⁻¹) q_e (mg g ⁻¹)	4.04×10^{-4} 111.11	0.95
Cd(II)	Pseudo first order	k_1 (min ⁻¹) q_e (mg g ⁻¹)	0.023 67.46	0.99
	Pseudo second order	k_2 (g mg ⁻¹ min ⁻¹) q_e (mg g ⁻¹)	1.7×10^{-3} 88.49	0.98

3.10. Adsorption Thermodynamics

The adsorption process of heavy metals onto solid adsorbents mainly takes place via electro-static forces so it is exothermic ($\Delta H < 0$) or endothermic ($\Delta H > 0$) in nature. The value of ΔH is the main parameter used to distinguish chemisorption from physisorption [47]. K_d is the equilibrium constant, showing free Gibbs energy (ΔG); consequently, the enthalpy (ΔH) and the entropy ΔS of adsorption could be calculated using the following equations:

$$\Delta G = -RT \ln k_d \quad (11)$$

$$\Delta G = \Delta H - T\Delta S \quad (12)$$

where T is the absolute temperature and R is the universal gas constant ($8.314 \text{ J mol}^{-1} \text{ K}^{-1}$). The plots of $\ln(K_d)$ vs. $1/T$ for Pb(II) and Cd(II) are shown, respectively, in Figure S9a,b in the Electronic Supplementary Materials (ESMs). The negative values of ΔG indicate the spontaneous nature of Pb(II) and Cd(II) adsorption onto EgLiCl-mGO. The positive values of ΔH demonstrate the endothermic character of the adsorption process, and ΔH more than 40 kJ mol^{-1} shows chemisorption and ΔH lower than 40 is related to chemisorption. The positive values of ΔS indicate the increase in disorder at the solid–liquid interface as well as more agitation in the sample solution due to releasing water molecules that grab the ions [48–50]. The obtained results are shown in Table 8.

Table 8. Thermodynamic parameters for the Pb(II) and Cd(II) adsorption onto EgLiCl-mGO.

T	Pb(II)			Cd(II)		
	C_e (mg L^{-1})	q_e (mg g^{-1})	ΔG (J mol^{-1})	C_e (mg L^{-1})	q_e (mg g^{-1})	ΔG (J mol^{-1})
273	28.65	6.75	3581	25.43	22.85	265
283	26.43	17.85	972	23.45	32.75	−827
298	22.91	35.45	−1081	20.85	45.75	−1946
318	14.65	76.75	−4103	17.76	61.2	−3065
343	7.13	114.35	−6875	12.21	88.95	−4920

4. Discussion

In the present study, a novel nanocomposite (EgLiCl-mGO) was successfully synthesized and applied as an efficient adsorbent in the MSPE procedure of Pb(II) and Cd(II) ions. The nanocomposite combining DES had the advantage of superparamagnetism, low environmental pollution, good water dispersibility, rapid extraction, and reproducibility; in the meantime, it showed excellent selectivity for Pb(II) and Cd(II). Moreover, its structural and magnetic properties were confirmed by FT-IR, VSM, and XRD. For the MSPE procedure, the affecting parameters on adsorption and desorption steps were optimized via the one-at-a-time method. LOD, LOQ, PF, EF, RSD, selectivity, effect of interference ions, selectivity, swelling behavior, isotherm adsorption, kinetic adsorption, and thermodynamic adsorption were investigated in detail. The technique was applied successfully to preconcentrate Pb(II) and Cd(II) simultaneously in four legume samples.

5. Conclusions

This article confirmed that EgLiCl-mGO is a qualified adsorbent to simultaneously preconcentrate ultratrace amounts of Pb(II) and Cd(II) in legumes. In addition to acceptable analytical results, this adsorbent is easy to prepare without consumption of dangerous and harmful reagents. The EgLiCl-mGO is an energy efficient and environmentally friendly adsorbent.

Supplementary Materials: The following supporting information can be downloaded at: <https://www.mdpi.com/article/10.3390/app13095702/s1>, This article includes Electronic Supplementary Materials (ESMs). FT-IR analysis, Effect of initial concentrations of **a** Pb(II) and **b** Cd(II) on adsorption capacity of EgLiCl-mGO, Langmuir model of **a** Pb(II) and **b** Cd(II) adsorptions onto EgLiCl-mGO, Freundlich model of **a** Pb(II) and **b** Cd(II) adsorptions onto EgLiCl-mGO, Temkin model of **a** Pb(II) and **b** Cd(II) adsorptions onto EgLiCl-mGO, Halsey model of **a** Pb(II) and **b** Cd(II) adsorptions onto EgLiCl-mGO, Elovich model of **a** Pb(II) and **b** Cd(II) adsorptions onto EgLiCl-mGO, the first-order kinetic model of **a** Pb(II) and **b** Cd(II) adsorptions onto EgLiCl-mGO, the first-order kinetic model of **a** Pb(II) and **b** Cd(II) adsorptions onto EgLiCl-mGO and thermodynamic parameters, enthalpy and entropy for the adsorption of **a** Pb(II) and **b** Cd(II) onto EgLiCl-mGO are provided in ESMs.

Author Contributions: Conceptualization: P.J. and M.H.; Methodology: P.J. and M.H.; Validation: P.J.; Formal Analysis: P.J. and M.H.; Investigation: P.J.; Resource: P.J. and M.H.; Data Curation: P.J.; Writing—Original Draft Preparation: P.J. and M.H.; Writing—Review and Editing: P.J. and M.H.; Supervision: P.J.; Project Administration: P.J. All authors have read and agreed to the published version of the manuscript.

Funding: This research received no external funding.

Institutional Review Board Statement: Not applicable.

Informed Consent Statement: Not applicable.

Data Availability Statement: The data presented in this study are available on request from the corresponding author.

Acknowledgments: Support for this study by the Research Council of the University of Tehran through grants is gratefully acknowledged.

Conflicts of Interest: The authors declare no conflict of interest.

References

1. Perna, F.M.; Vitale, P.; Capriati, V. Deep eutectic solvents and their applications as green solvents. *Curr. Opin. Green Sustain. Chem.* **2020**, *21*, 27–33. [[CrossRef](#)]
2. Socas-Rodríguez, B.; Torres-Cornejo, M.V.; Álvarez-Rivera, G.; Mendiola, J.A. Deep Eutectic Solvents for the Extraction of Bioactive Compounds from Natural Sources and Agricultural By-Products. *Appl. Sci.* **2021**, *11*, 4897. [[CrossRef](#)]
3. Hansen, B.B.; Spittle, S.; Chen, B.; Poe, D.; Zhang, Y.; Klein, J.M.; Horton, A.; Adhikari, L.; Zelovich, T.; Doherty, B.W.; et al. Deep Eutectic Solvents: A Review of Fundamentals and Applications. *Chem. Rev.* **2021**, *121*, 1232–1285. [[CrossRef](#)]
4. Moura, L.; Moufawad, T.; Ferreira, M.; Bricout, H.; Tilloy, S.; Monflier, E.; Costa Gomes, M.F.; Landy, D.; Fourmentin, S. Deep eutectic solvents as green absorbents of volatile organic pollutants. *Environ. Chem. Lett.* **2017**, *15*, 747–753. [[CrossRef](#)]
5. Rodríguez-Ramos, R.; Santana-Mayor, Á.; Socas-Rodríguez, B.; Rodríguez-Delgado, M.Á. Recent Applications of Deep Eutectic Solvents in Environmental Analysis. *Appl. Sci.* **2021**, *11*, 4779. [[CrossRef](#)]
6. Alomar, T.S.; Habila, M.A.; AlMasou, N.; Alothman, Z.A.; Sheikh, M.; Soyak, M. Biomass-Derived Adsorbent for Dispersive Solid-Phase Extraction of Cr(III), Fe(III), Co(II) and Ni(II) from Food Samples Prior to ICP-MS Detection. *Appl. Sci.* **2021**, *11*, 7792. [[CrossRef](#)]
7. Plastiras, O.E.; Deliyanni, E.; Samanidou, V. Synthesis and Application of the Magnetic Nanocomposite GO-Chm for the Extraction of Benzodiazepines from Surface Water Samples Prior to HPLC-PDA Analysis. *Appl. Sci.* **2021**, *11*, 7828. [[CrossRef](#)]
8. Hejazi Khah, M.; Jamshidi, P.; Shemirani, F. Applying Fe₃O₄-MoS₂-chitosan nanocomposite to preconcentrate heavy metals from dairy products prior quantifying by FAAS. *Res. Chem. Intermed.* **2021**, *47*, 3867–3881. [[CrossRef](#)]
9. Bhaskar, S.; Visweswar Kambhampati, N.S.; Ganesh, K.M.; Sharma, P.M.; Srinivasan, V.; Ramamurthy, S.S. Metal-Free, Graphene Oxide-Based Tunable Soliton and Plasmon Engineering for Biosensing Applications. *ACS Appl. Mater. Interfaces* **2021**, *13*, 17046–17061. [[CrossRef](#)]
10. Rai, A.; Bhaskar, S.; Ganesh, K.M.; Ramamurthy, S.S. Engineering of coherent plasmon resonances from silver soret colloids, graphene oxide and Nd₂O₃ nanohybrid architectures studied in mobile phone-based surface plasmon-coupled emission platform. *Mater. Lett.* **2021**, *304*, 130632. [[CrossRef](#)]
11. Khalilifard, M.; Javadian, S. Magnetic superhydrophobic polyurethane sponge loaded with Fe₃O₄@oleic acid@graphene oxide as high performance adsorbent oil from water. *Chem. Eng. J.* **2021**, *408*, 127369. [[CrossRef](#)]
12. Khawaja, H.; Zahir, E.; Asghar, M.A.; Asghar, M.A. Graphene oxide decorated with cellulose and copper nanoparticle as an efficient adsorbent for the removal of malachite green. *Int. J. Biolog. Macromol.* **2021**, *167*, 23–34. [[CrossRef](#)] [[PubMed](#)]

13. Ibrahim, R.K.; El-Shafie, A.; Hin, L.S.; Mohd, N.S.B.; Aljumaily, M.M.; Ibraim, S.; AlSaadi, M.A. A clean approach for functionalized carbon nanotubes by deep eutectic solvents and their performance in the adsorption of methyl orange from aqueous solution. *J. Environ. Manag.* **2019**, *235*, 521–534. [[CrossRef](#)] [[PubMed](#)]
14. Wang, X.; Li, G.; Row, K.H. Graphene and Graphene Oxide Modified by Deep Eutectic Solvents and Ionic Liquids Supported on Silica as Adsorbents for Solid-Phase Extraction. *Bull. Korean Chem. Soc.* **2017**, *38*, 251–257. [[CrossRef](#)]
15. Lomba, L.; García, C.B.; Ribate, M.P.; Giner, B.; Zuriaga, E. Applications of Deep Eutectic Solvents Related to Health, Synthesis, and Extraction of Natural Based Chemicals. *Appl. Sci.* **2021**, *11*, 10156. [[CrossRef](#)]
16. Kamel, A.H.; Amr, A.E.G.E.; Al-Omar, M.A.; Elsayed, A.E. Pre-Concentration Based on Cloud Point Extraction for Ultra-Trace Monitoring of Lead (II) Using Flame Atomic Absorption Spectrometry. *Appl. Sci.* **2019**, *9*, 4752. [[CrossRef](#)]
17. Alotaibi, K.M.; Almethen, A.A.; Beagan, A.M.; Al-Swaidan, H.M.; Ahmad, A.; Bhawani, S.A.; Alswieleh, A.M. Quaternization of Poly(2-diethyl aminoethyl methacrylate) Brush-Grafted Magnetic Mesoporous Nanoparticles Using 2-Iodoethanol for Removing Anionic Dyes. *Appl. Sci.* **2021**, *11*, 10451. [[CrossRef](#)]
18. Wang, S.; Li, X.; Li, M.; Li, X.; Li, X.; Li, S.; Zhang, Q.; Li, H. Self-Assembled Three-Dimensional Microporous rGO/PNT/Fe₃O₄ Hydrogel Sorbent for Magnetic Preconcentration of Multi-Residue Insecticides. *Appl. Sci.* **2020**, *10*, 5665. [[CrossRef](#)]
19. Huang, X.; Liu, G.; Xu, D.; Xu, X.; Li, L.; Zheng, S.; Lin, H.; Gao, H. Novel Zeolitic Imidazolate Frameworks Based on Magnetic Multiwalled Carbon Nanotubes for Magnetic Solid-Phase Extraction of Organochlorine Pesticides from Agricultural Irrigation Water Samples. *Appl. Sci.* **2018**, *8*, 959. [[CrossRef](#)]
20. Jamshidi, P.; Shemirani, F. Adsorption/desorption of acid violet-7 onto magnetic MnO₂ prior to its quantification by UV-visible spectroscopy: Optimized by fractional factorial design. *Res. Chem. Intermed.* **2020**, *46*, 4403–4422. [[CrossRef](#)]
21. Nishina, Y.; Eigler, S. Chemical and electrochemical synthesis of graphene oxide—a generalized view. *Nanoscale* **2020**, *12*, 12731–12740. [[CrossRef](#)] [[PubMed](#)]
22. Sujiono, E.H.; Zabrian, D.; Dahlan, M.; Amin, B.; Agus, J. Graphene oxide based coconut shell waste: Synthesis by modified Hummers method and characterization. *Heliyon* **2020**, *6*, e04568. [[CrossRef](#)] [[PubMed](#)]
23. Dana, M.; Jamshidi, P.; Shemirani, F. Acid Brown-14 preconcentration onto an adsorbent consisting of Fe₃O₄, carbon nanotube and CeO: Optimized by a multi-variable method. *Res. Chem. Intermed.* **2021**, *47*, 1021–1032. [[CrossRef](#)]
24. Hejazi Khah, M.; Jamshidi, P.; Shemirani, F. Applicability of an eco-friendly deep eutectic solvent loaded onto magnetic graphene oxide to preconcentrate trace amount of indigotin blue dye. *J. Mol. Liq.* **2021**, *342*, 117346. [[CrossRef](#)]
25. Workie, Y.A.; Sabrina Imae, T.; Krafft, M.P. Nitric oxide gas delivery by fluorinated poly (Ethylene Glycol)@ graphene oxide carrier toward pharmacotherapeutics. *ACS Biomater. Sci. Eng.* **2019**, *5*, 2926–2934. [[CrossRef](#)]
26. Majid, F.; Ali, M.D.; Ata, S.; Bibi, I.; Malik, A.; Ali, A.; Alwadai, N.; Albalawi, H.; Shoab, M.; Bukhari, S.A.; et al. Fe₃O₄/graphene oxide/Fe₄[Fe(CN)₆]₃ nanocomposite for high performance electromagnetic interference shielding. *Ceram. Int.* **2021**, *47*, 11587–11595. [[CrossRef](#)]
27. Ma, Z.; Guan, Y.; Liu, H. Synthesis and characterization of micron-sized monodisperse superparamagnetic polymer particles with amino groups. *J. Polym. Sci. A Polym. Chem.* **2005**, *43*, 3433–3439. [[CrossRef](#)]
28. Faryadras, F.; Yousefi, S.M.; Jamshidi, P.; Shemirani, F. Application of magnetic graphene-based bucky gel as an efficient green sorbent for determination of mercury in fish and water samples. *Res. Chem. Intermed.* **2020**, *46*, 2055–2068. [[CrossRef](#)]
29. Zhang, J.; Wang, L.; Wang, A. Preparation and Properties of Chitosan-g-poly(acrylic acid)/Montmorillonite Superabsorbent Nanocomposite via in Situ Intercalative Polymerization. *Ind. Eng. Chem. Res.* **2007**, *46*, 2497–2502. [[CrossRef](#)]
30. Shuyue, J.; Dongyan, T.; Jing, P.; Xu, Y.; Zhaojie, S. Crosslinked electrospinning fibers with tunable swelling behaviors: A novel and effective adsorbent for Methylene Blue. *Chem. Eng. J.* **2020**, *390*, 124472. [[CrossRef](#)]
31. Jamshidi, P.; Alvand, M.; Shemirani, F. Magnetic Mn₂O₃ nanocomposite covered with N,N'-bis(salicylidene)ethylenediamine for selective preconcentration of cadmium(II) prior to its quantification by FAAS. *Microchim. Acta* **2019**, *186*, 487. [[CrossRef](#)] [[PubMed](#)]
32. Fei, J.J.; Zhao, L.Y.; Wu, X.H.; Cui, X.B.; Min, H.; Lian, H.Z.; Chen, Y.J. In-tube solid-phase microextraction with a hybrid monolithic column for the preconcentration of ultra-trace metals prior to simultaneous determination by ICP-MS. *Microchim. Acta* **2020**, *187*, 356. [[CrossRef](#)] [[PubMed](#)]
33. Kobylinska, N.; Kostenko, L.; Khainakov, S.; Garcia-Granda, S. Advanced core-shell EDTA-functionalized magnetite nanoparticles for rapid and efficient magnetic solid phase extraction of heavy metals from water samples prior to the multi-element determination by ICP-OES. *Microchim. Acta* **2020**, *187*, 289. [[CrossRef](#)] [[PubMed](#)]
34. Sorouraddin, S.M.; Farajzadeh, M.A.; Dastoori, H. Development of a dispersive liquid-liquid microextraction method based on a ternary deep eutectic solvent as chelating agent and extraction solvent for preconcentration of heavy metals from milk samples. *Talanta* **2020**, *208*, 120485. [[CrossRef](#)] [[PubMed](#)]
35. Shirani, M.; Salari, F.; Habibollahi, S.; Akbari, A. Needle hub in-syringe solid phase extraction based a novel functionalized biopolyamide for simultaneous green separation/preconcentration and determination of cobalt, nickel, and chromium (III) in food and environmental samples with micro sampling flame atomic absorption spectrometry. *Microchem. J.* **2020**, *152*, 104340.
36. Ozdemir, S.; Kiliç, E.; Acer, Ö.; Soyvak, M. Simultaneous preconcentrations of Cu(II), Ni(II), and Pb(II) by SPE using E. profundum loaded onto Amberlite XAD-4. *Microchem. J.* **2021**, *171*, 106758. [[CrossRef](#)]
37. Jamshidi, P.; Shemirani, F. Adsorption and desorption of Pb²⁺ on magnetic Mn₂O₃ as highly efficient adsorbent: Isotherm, kinetic and thermodynamic studies. *Colloids Surf. A Physicochem. Eng. Asp.* **2019**, *571*, 151–159. [[CrossRef](#)]

38. Brdar, M.; Šćiban, M.; Takači, A.; Došenović, T. Comparison of two and three parameters adsorption isotherm for Cr(VI) onto Kraft lignin. *Chem. Eng. J.* **2012**, *183*, 108–111. [[CrossRef](#)]
39. Nait-Merzoug, A.; Guellati, O.; Djaber, S.; Habib, N.; Harat, A.; El-Haskouri, J.; Begin, D.; Guerioune, M. Ni/Zn Layered Double Hydroxide (LDH) Micro/Nanosystems and Their Azorubine Adsorption Performance. *Appl. Sci.* **2021**, *11*, 8899. [[CrossRef](#)]
40. Rajahmundry, G.K.; Garlapati, C.; Kumar, P.S.; Alwi, R.S.; Vo, D.V.N. Statistical analysis of adsorption isotherm models and its appropriate selection. *Chemosphere* **2021**, *276*, 130176. [[CrossRef](#)]
41. Jamshidi, P.; Shemirani, F. Synthesis of a magnetic WO₃ nanocomposite for use in highly selective preconcentration of Pb(II) prior to its quantification by FAAS. *Microchim. Acta* **2018**, *185*, 421. [[CrossRef](#)] [[PubMed](#)]
42. Tejada-Tovar, C.; Villabona-Ortíz, Á.; Gonzalez-Delgado, D. Removal of Nitrate Ions Using Thermally and Chemically Modified Bioadsorbents. *Appl. Sci.* **2021**, *11*, 8455. [[CrossRef](#)]
43. Ukkund, S.J.; Puthiyillam, P.; Alshehri, H.M.; Goodarzi, M.; Taqui, S.N.; Anqi, A.E.; Safaei, M.R.; Ali, M.A.; Syed, U.T.; Mir, R.A.; et al. Adsorption Method for the Remediation of Brilliant Green Dye Using Halloysite Nanotube: Isotherm, Kinetic and Modeling Studies. *Appl. Sci.* **2021**, *11*, 8088. [[CrossRef](#)]
44. Singh, S.; Kapoor, D.; Khasnabis, S.; Singh, J.; Ramamurthy, P.C. Mechanism and kinetics of adsorption and removal of heavy metals from wastewater using nanomaterials. *Environ. Chem. Lett.* **2021**, *19*, 2351–2381. [[CrossRef](#)]
45. Ighalo, J.O.; Adeniyi, A.G.; Eletta, O.A.A.; Arowoyele, L.T. Competitive adsorption of Pb(II), Cu(II), Fe(II) and Zn(II) from aqueous media using biochar from oil palm (*Elaeis guineensis*) fibers: A kinetic and equilibrium study. *Indian Chem. Eng.* **2021**, *63*, 501–511. [[CrossRef](#)]
46. Zhang, X.; Yan, L.; Li, J.; Yu, H. Adsorption of heavy metals by l-cysteine intercalated layered double hydroxide: Kinetic, isothermal and mechanistic studies. *J. Colloid Interface Sci.* **2020**, *562*, 149–158. [[CrossRef](#)]
47. Abbou, B.; Lebdiri, I.; Ouaddari, H.; Kadiri, L.; Ouass, A.; Habssaoui, A.; Lebdiri, A.; El Housseine, R. Removal of Cd (II), Cu (II), and Pb (II) by adsorption onto natural clay: A kinetic and thermodynamic study. *Turk. J. Chem.* **2021**, *45*, 362–376. [[CrossRef](#)]
48. Nistor, M.A.; Muntean, S.G.; Ianoș, R.; Racoviceanu, R.; Ianași, C.; Cseh, L. Adsorption of Anionic Dyes from Wastewater onto Magnetic Nanocomposite Powders Synthesized by Combustion Method. *Appl. Sci.* **2021**, *11*, 9236. [[CrossRef](#)]
49. Abbas, M.; Trari, M. Kinetic, equilibrium and thermodynamic study on the removal of Congo Red from aqueous solutions by adsorption onto apricot stone. *Process. Saf. Environ. Prot.* **2015**, *98*, 424–436. [[CrossRef](#)]
50. Nadarajah, K.; Bandala, E.R.; Zhang, Z.; Mundree, S.; Goonetilleke, A. Removal of heavy metals from water using engineered hydrochar: Kinetics and mechanistic approach. *J. Water Process. Eng.* **2021**, *40*, 101929. [[CrossRef](#)]